ANTIOXIDANTS & REDOX SIGNALING
Volume 23, Number 16, 2015

DOI: 10.1089/ars.2014.6108

Discoveries

ORIGINAL RESEARCH COMMUNICATION

Myeloperoxidase–Hepatocyte–Stellate Cell Cross Talk Promotes Hepatocyte Injury and Fibrosis in Experimental Nonalcoholic Steatohepatitis

Benjamin Pulli,[1,2] Muhammad Ali,[1] Yoshiko Iwamoto,[1] Matthias W.G. Zeller,[1] Stefan Schob,[1] Jenny J. Linnoila,[1] and John W. Chen[1,2]

Abstract

Aims: Myeloperoxidase (MPO), a highly oxidative enzyme secreted by leukocytes has been implicated in human and experimental nonalcoholic steatohepatitis (NASH), but the underlying mechanisms remain unknown. In this study, we investigated how MPO contributes to progression from steatosis to NASH. ***Results:*** In C57Bl/6J mice fed a diet deficient in methionine and choline to induce NASH, neutrophils and to a lesser extent inflammatory monocytes are markedly increased compared with sham mice and secrete abundant amounts of MPO. Through generation of HOCl, MPO directly causes hepatocyte death *in vivo*. *In vitro* experiments demonstrate mitochondrial permeability transition pore induction *via* activation of SAPK/JNK and PARP. MPO also contributes to activation of hepatic stellate cells (HSCs), the most important source of collagen in the liver. *In vitro* MPO-activated HSCs have an activation signature (MAPK and PI3K-AKT phosphorylation) and upregulate *COL1A1*, *α-SMA*, and *CXCL1*. MPO-derived oxidative stress also activates transforming growth factor *β* (TGF-*β*) *in vitro*, and TGF-*β* signaling inhibition with SB-431542 decreased steatosis and fibrosis *in vivo*. Conversely, congenital absence of MPO results in reduced hepatocyte injury, decreased levels of TGF-*β*, fewer activated HSCs, and less severe fibrosis *in vivo*. ***Innovation and Conclusion:*** Cumulatively, these findings demonstrate important cross talk between inflammatory myeloid cells, hepatocytes, and HSCs *via* MPO and establish MPO as part of a proapoptotic and profibrotic pathway of progression in NASH, as well as a potential therapeutic target to ameliorate this disease. *Antioxid. Redox Signal.* 23, 1255–1269.

Introduction

NONALCOHOLIC FATTY LIVER disease (NAFLD) is the most common liver disease in Western society (6). While steatosis is a relatively benign condition with only 1.5% of patients progressing to fibrosis/cirrhosis (1), 30–50% patients with nonalcoholic steatohepatitis (NASH) progress (13, 14). However, the role of leukocyte subsets and their derivatives remains unclear because they can have both pro- and anti-fibrotic properties (12). Several key scenarios that promote progression to fibrosis have been discovered: (i) hepatocyte injury distinguishes progressive from nonprogressive NAFLD (31), (ii) hepatocyte apoptosis leads to fibrosis (49), (iii) TGF-*β* is a crucial profibrotic cytokine (19), (iv) hepatic stellate cells (HSCs) are the main collagen-producing cells in

Innovation

Nonalcoholic fatty liver disease (NAFLD) is the most common liver disease in western society, but it remains unknown what factors trigger progression to nonalcoholic steatohepatitis (NASH). Myeloperoxidase (MPO) is an important oxidative enzyme, and increased MPO concentrations were previously found in human NASH compared with steatosis. In our murine NASH model, MPO contributes to hepatocyte injury, activates hepatic stellate cells, and promotes fibrosis. Therefore, MPO could also be both an attractive biomarker and a therapeutic target to prevent the development of hepatocyte injury and fibrosis in NAFLD.

[1]Center for Systems Biology, Massachusetts General Hospital and Harvard Medical School, Boston, Massachusetts.
[2]Department of Radiology, Massachusetts General Hospital, Boston, Massachusetts.

the liver (16), and (v) oxidative stress markers correlate with NAFLD severity (45).

Myeloperoxidase (MPO) is the most abundant and highly oxidizing inflammatory enzyme contained in neutrophil and monocyte granules (24). Unlike other oxidizing enzymes (*e.g.*, NADPH oxidase), in the liver, it is only expressed in myeloid cells (3). In an environment with high levels of hepatocyte-derived H_2O_2 and other reactive oxygen species (ROS), secreted MPO could potentiate oxidative stress and tissue damage by forming hypochlorous acid (HOCl) from hydrogen peroxide (H_2O_2) and also reactive nitrogen species from nitrite or nitric oxide (24). Recently, it was reported that human livers with NASH contain higher amounts of MPO compared with steatotic specimens (41), and that chimeric *LDLR*$^{-/-}$ mice with an MPO-deficient hematopoietic system have decreased inflammation and fibrosis in a high-fat diet-induced disease model of NASH (40). However, how MPO acts to influence progression and fibrosis in NASH remains unknown.

In this study, we show that MPO participates in several key scenarios that promote progression to fibrosis. MPO potentiates oxidative stress and causes hepatocyte injury *in vitro* and *in vivo*. Surprisingly, MPO-derived oxidative stress activates transforming growth factor β (TGF-β) and HSCs, the main source of collagen production in the liver (16), and MPO-activated HSCs in turn secrete CXCL1. In line with this, congenitally MPO-deficient NASH mice have greatly reduced HSC activation, fibrosis, and hepatocyte injury. Thus, MPO provides an important link between inflammatory myeloid cells, hepatocytes, and HSCs to promote hepatocyte death and fibrosis in NASH.

Results

MPO expression and activity are increased in NASH, and MPO is mostly expressed and secreted by neutrophils

We fed C57BL/6J wild-type (WT) mice a methionine and choline-deficient (MCD) diet to induce NASH (54). First, we evaluated the proportion and cell numbers of myeloid cells in the liver of these mice with flow cytometry. Neutrophils were markedly increased in the liver of NASH mice (Fig. 1a). Inflammatory Ly-6C^{high} monocytes and Kupffer cells were also increased, although to a lesser extent. The marked increase in neutrophils was confirmed on histology (Supplementary Fig. S1a; Supplementary Data are available online at www.liebertpub.com/ars), and neutrophils are the most elevated myeloid cell type both in relative and absolute numbers (Fig. 1a, b). Immunohistochemistry for MPO revealed that MPO-positive cells were significantly increased in NASH (Fig. 1c).

On immunofluorescence, most MPO-expressing cells colocalized with Ly-6G-positive cells (Supplementary Fig. S1b). MPO protein (as determined by ELISA) and MPO activity were also markedly elevated (Fig. 1d). Flow cytometry confirmed the increase in MPO-expressing cells (Supplementary Fig. S1c). There has been debate about the cellular source of MPO in NASH (3, 41). Our results indicate that in NASH, approximately 87% of MPO was secreted by neutrophils and 13% was secreted by Ly-6C^{high} monocytes (Supplementary Fig. S1c). Additionally, the percentage of MPO-positive neutrophils was increased in NASH (Fig. 1e).

These experiments identify neutrophils and inflammatory monocytes as the most important sources of MPO in NASH. Kupffer cells, dendritic cells, and Ly-6C^{low} monocytes do not have significant amounts of MPO in their cytoplasm. To cause oxidative stress outside of myeloid cells in the liver, MPO needs to be secreted into the extracellular space. To confirm this, we isolated liver extracellular protein fractions (34). Extracellular MPO activity was significantly increased in wild-type (WT) NASH *versus* MPO knockout (MPO$^{-/-}$) NASH and sham mice (Fig. 1f).

MPO$^{-/-}$ mice have less severe steatohepatitis and fibrosis compared with wild-type controls

To clarify if MPO is merely a bystander or whether it plays a pathogenic role in NASH, we compared NASH severity markers in WT and MPO knockout (MPO$^{-/-}$) mice fed an MCD diet to induce NASH. Masson's trichrome staining revealed typical, chicken-wire distributed incipient fibrosis in WT mice, while less fibrosis and less liver hydroxyproline were detected in MPO$^{-/-}$ mice (Fig. 2a, b). MPO$^{-/-}$ mice also had decreased steatosis (quantified on histology as well as per Oil Red O, Fig. 2c) and less hepatocyte injury, with fewer ballooning cells compared with WT controls, and a lower NAFLD activity score (NAS) (Fig. 2d), consistent with significantly less severe histological steatohepatitis. To confirm this difference, we also analyzed inflammatory and fibrotic gene expression by real time-polymerase chain reaction RT-PCR.

Corroborating our histology findings, we detected lower levels of the fibrosis markers, *COL1A1* and tissue inhibitor of metalloproteinase 1 (*TIMP-1*), as well as lower levels of the inflammatory markers, *TNF* and *IL-1β*, in MPO$^{-/-}$ mice, while no difference was detected in *IL-10* levels (Fig. 2e). To investigate effects of MPO on visceral adipose tissue and function of the intestinal barrier, we measured adiponectin levels in serum and visceral fat, as well as endotoxin levels in serum and liver. However, we did not find significant differences between WT and MPO$^{-/-}$ NASH mice (Fig. 2f). To exclude effects of methionine and choline deficiency on neutrophil function, we isolated neutrophils from mice fed the MCD diet for 1 week and control mice and stimulated them *in vitro*. There, we did not find a difference in MPO secretion or oxidative burst formation (as evaluated by superoxide anion production) (Supplementary Fig. S1d).

MPO induces hepatocyte death in vitro *and* in vivo

On histology, MPO$^{-/-}$ NASH mice had less severe hepatocyte injury compared with WT NASH mice (Fig. 2a, c). To confirm this finding, we injected the membrane-impermeable DNA dye, Sytox Red, intravenously into WT and MPO$^{-/-}$ mice with NASH. On fluorescence microscopy (Fig. 3a) and flow cytometry (Fig. 3b), we detected more Sytox Red-positive (late apoptotic/necrotic) liver cells in wild-type than in MPO$^{-/-}$ mice. In addition, we detected colocalization of Sytox Red-positive cells with MPO on immunofluorescence (Fig. 3c). To further establish a potential direct effect of MPO on hepatocyte injury, we incubated hepatocytes with different concentrations of MPO and GOX (as an H_2O_2 donor). In line with our hypothesis, increasing concentrations of MPO-potentiated oxidative stress caused by GOX-derived H_2O_2 resulted in rapid hepatocyte death, as evidenced by propidium iodide (PI) uptake (Fig. 3d).

Because MPO can activate matrix metalloproteinases (MMPs) (43) and both MMPs and TGF-β have been shown to

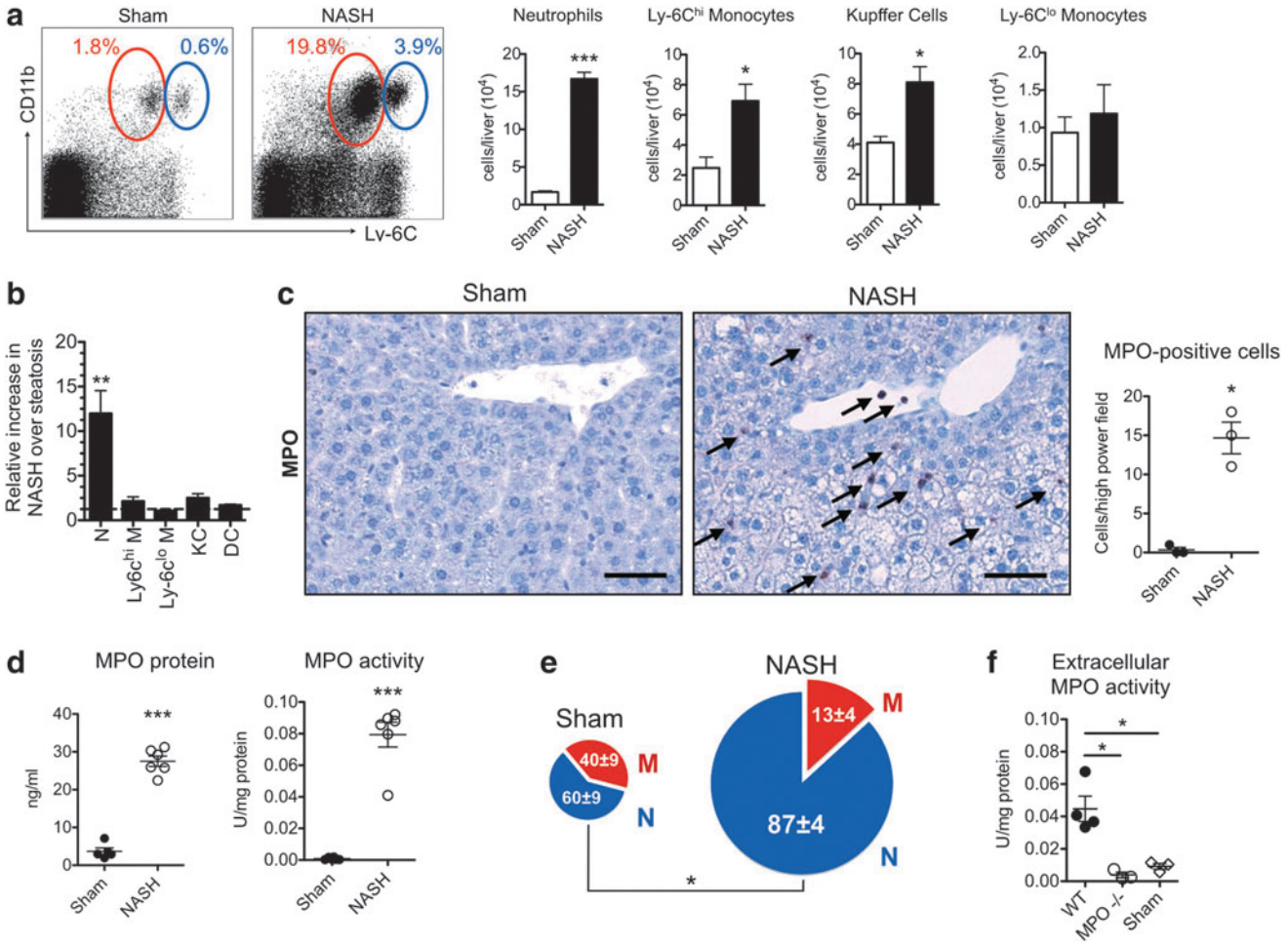

FIG. 1. Myeloperoxidase (MPO)-expressing cells, MPO protein, and MPO activity are increased in nonalcoholic steatohepatitis (NASH). (a) Flow cytometric analysis of liver myeloid cells in NASH: neutrophils (*red gate*) and inflammatory Ly-6C^{high} monocytes (*blue gate*) ($n=5$ per group). **(b)** Relative fold increase of different myeloid cell populations in NASH over sham ($n=5$ per group). **(c)** Immunohistochemistry for MPO in NASH compared with sham mice (*arrows* indicate MPO positive cells, bar = 50 μm, $n=3$ per group). **(d)** Liver MPO protein and MPO activity ($n=5$–6 per group). **(e)** Pie chart of MPO-expressing cells as quantified by flow cytometry. Overall pie chart size reflects the absolute numbers of MPO-positive cells per liver, while numbers in pie chart reflect the percentages of cell types ($n=4$–5 per group). **(f)** Extracellular fluid MPO activity in wild-type (WT) and MPO knockout (MPO$^{-/-}$) NASH mice compared with sham mice ($n=3$–4 per group). All data are mean ± SEM. Lin = CD90/CD49.2/B220/NK1.1/Ly-6G. $*p<0.05$, $**p<0.01$, $***p<0.001$. KC, Kupffer cells; DC, dendritic cells; N, neutrophils; M, monocytes. To see this illustration in color, the reader is referred to the web version of this article at www.liebertpub.com/ars

induce hepatocyte apoptosis (19, 22), we preincubated isolated hepatocytes with ABAH (an irreversible MPO inhibitor), taurine (an HOCl scavenger), marimastat (a pan-MMP inhibitor), SB-431542 (a TGF-β signaling inhibitor), or a protease inhibitor cocktail before addition of MPO and GOX. Both ABAH and taurine diminished MPO-induced hepatocyte death, while no effect from marimastat, SB-431542, or protease inhibitor was seen (Fig. 4a).

To further investigate the intracellular pathways involved, we performed an intracellular signaling array, where we detected increased phosphorylation of AMPK, JNK, and rpS6, as well as increased cleavage of PARP (Fig. 4b). These findings were confirmed on Western blotting, where we found increased phosphorylation of AMPK and JNK with MPO compared with vehicle or GOX-treated hepatocytes (Fig. 4c). Caspase-3 cleavage was not affected and this was confirmed with a caspase 3/7 activity assay (Fig. 4c). Similarly, no differences in phosphorylation of p38 (Fig. 4c) and no differences of phosphorylated or unphosphorylated Stat1 (Supplementary Fig. S2a) were detected on Western blots, validating the results of the signaling array. Since both JNK and PARP have been implicated in mitochondrial permeability transition (MPT) (2, 50), we tested if cyclosporine A, an inhibitor of MPT, affects MPO-induced cell death. Indeed, we observed a marked reduction in cell death with cyclosporine A compared with vehicle (Fig. 4d).

Healthy hepatocytes have high antioxidative capacity (21), which should in theory protect them against MPO-mediated ROS. In NAFLD, this capacity is compromised (39), which may render hepatocytes more susceptible to damage. We therefore isolated hepatocytes from both control and NASH mice to investigate differences in susceptibility to MPO. Indeed, we found that hepatocytes from NASH mice underwent cell death at lower MPO concentrations compared with

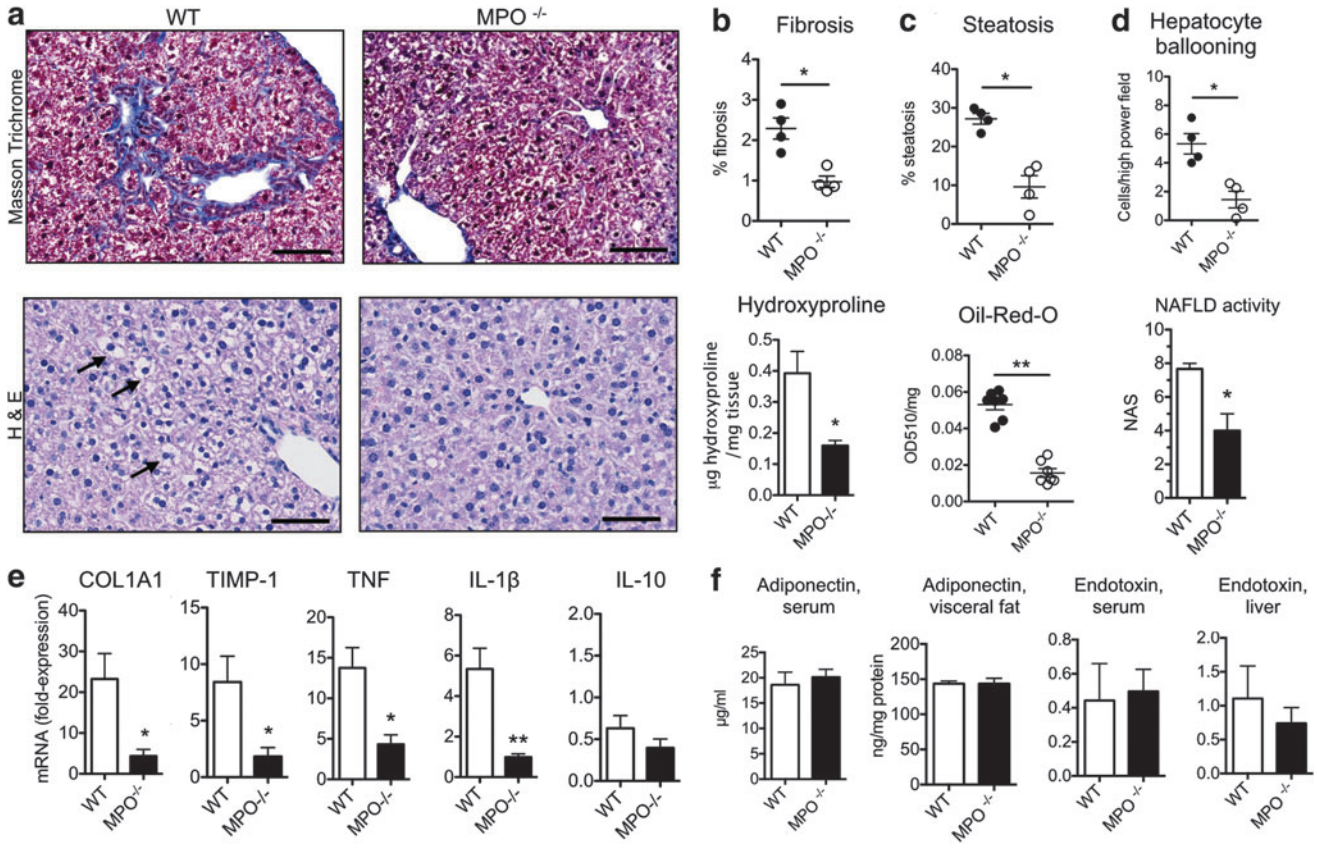

FIG. 2. MPO deficiency attenuates the severity of fibrosis and hepatocyte injury. (a) Masson's trichrome (*top row*) and hematoxylin and eosin (H&E, *bottom row*) staining of liver sections of wild-type (WT) and MPO knockout ($MPO^{-/-}$) NASH mice. In the *top row*, collagen is stained in *blue*; in the *bottom row*, hepatocyte ballooning is marked with *arrows* (bars = 50 μm). **(b)** Quantification of fibrosis on histology ($n = 4$ per group) and with hydroxyproline assay ($n = 6$ per group). **(c)** Quantification of steatosis on histology and on Oil Red O assay ($n = 4$–6 per group). **(d)** Quantification of hepatocyte ballooning and NAFLD activity score (NAS, $n = 4$ per group) **(e)** real time (RT)-polymerase chain reaction mRNA quantification of *COL1A1*, *TIMP-1*, *TNF*, *IL-1β*, and *IL-10* relative to sham mice ($n = 6$ per group). **(f)** Adiponectin in serum and visceral fat, as well as endotoxin in serum and liver as determined by ELISA as well as biochemical assay, respectively. All data are mean ± SEM. $^*p < 0.05$, $^{**}p < 0.01$. To see this illustration in color, the reader is referred to the web version of this article at www.liebertpub.com/ars

hepatocytes from control mice (Fig. 4e), further establishing a role for MPO in hepatocyte death in NASH.

MPO activates HSCs

Activated HSCs are a significant source of collagen and are crucial for the progression of NASH (16). In cultured primary HSCs incubated with different concentrations of MPO, we found that MPO-activated HSCs upregulated α-smooth muscle actin [α-*SMA*, a well-established marker for HSC activation (16)] and *COL1A1* (which encodes the main component of type I collagen) mRNA in a dose-dependent manner (Fig. 5a). Because both TGF-β and MMPs are known to activate HSCs (19, 33) and MPO can activate MMPs (43), we investigated the role of these molecules in MPO-mediated HSC activation. The dose-dependent increase in α-*SMA* and *COL1A1* expression in HSCs after stimulation with MPO was abrogated by ABAH and taurine (Fig. 5a), indicating an HOCl-mediated effect. Inhibiting MMPs with marimastat also diminished the response of HSCs to MPO, and TGF-β signaling inhibition with SB431542 partially inhibited the response to MPO (Fig. 5a).

To test the activity of SB-431542, we cultured HSCs for 5 days in the presence of this inhibitor [when cultured *in vitro* for several days, HSCs spontaneously activate *via* TGF-β signaling (4)] and found markedly decreased *COL1A1* expression, consistent with successful TGF-β signaling inhibition (Supplementary Fig. S2b). Importantly, only ABAH directly inhibited MPO activity, and only ABAH and taurine decreased HOCl production by MPO, excluding direct effects of marimastat or SB431542 on the MPO enzyme (Supplementary Fig. S2c). On intracellular signaling array, a significant increase in phosphorylation of Akt, the 70-kDa ribosomal protein S6 kinase (P70S6K), extracellular signal-regulated kinases (ERK), and JNK, as well as decreased cleavage of PARP and decreased phosphorylation of PRAS40 were found in MPO-activated HSCs (Fig. 5b). This is consistent with activation of the profibrotic and proliferative PIP3/Akt/P70S6K and MAPK (ERK/JNK) pathways in HSCs (17, 26, 29, 37, 38). Applying these findings to NASH, we observed fewer activated HSCs, as shown by reduced α-SMA staining and mRNA. (Fig. 5c), but more vitamin A-containing quiescent HSCs (28) in $MPO^{-/-}$ compared with WT mice on flow cytometry (Fig. 5d).

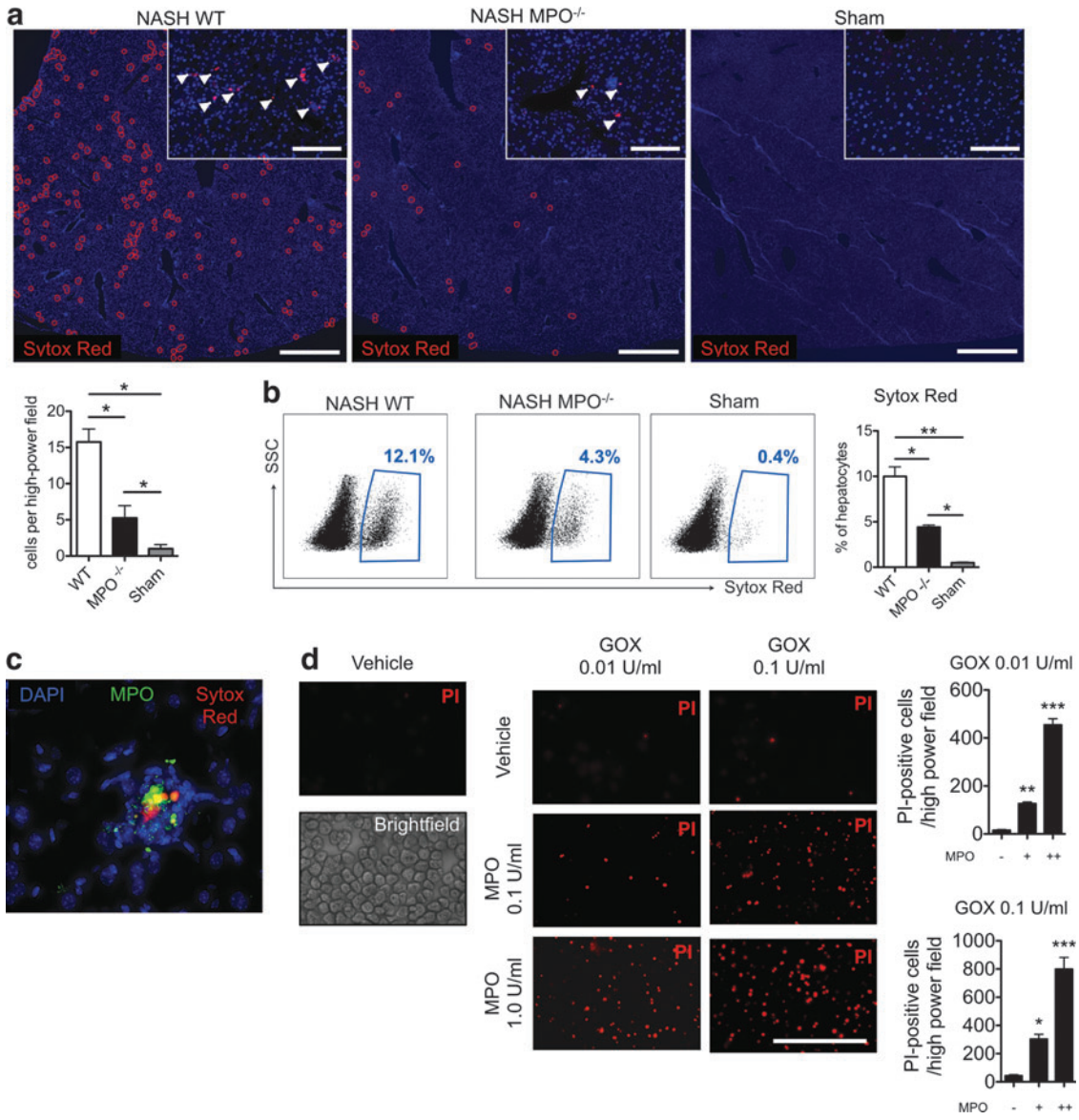

FIG. 3. MPO directly contributes to hepatocyte death *in vivo* and *in vitro*. Liver immunofluorescence **(a)** and flow cytometry **(b)** of Sytox Red-labeled hepatocytes in wild-type (WT) and MPO knockout ($MPO^{-/-}$) NASH and sham mice ($n=4$ per group, *arrowheads* indicate Sytox Red positive cells, bar in low magnification represents 1 mm, bar in high magnification represents 50 μm, *blue* counterstain is DAPI). **(c)** Liver immunofluorescence in NASH mice for MPO (anti-MPO, *green*) and injured hepatocytes (Sytox Red, *red*, counterstain is DAPI, bar = 50 μm). **(d)** Cell death (propidium iodide, PI) in primary hepatocytes (bright-field panel) cultured in the presence of MPO and glucose oxidase (GOX) ($n=4$ per group, bar = 100 μm). $^{*}p<0.05$, $^{**}p<0.01$, $^{***}p<0.001$. To see this illustration in color, the reader is referred to the web version of this article at www.liebertpub.com/ars

To evaluate the importance of MPO compared with other molecules secreted by activated neutrophils, we cocultured neutrophils and HSCs. N-formylmethionyl-leucyl-phenylalanine (fMLP)-activated neutrophils increased *COL1A1* and α-*SMA* expression in HSCs and ABAH partially inhibited this effect (Supplementary Fig. S2e). MPO activity and inhibition by ABAH were confirmed in the supernatant from the coculture experiment (Supplementary Fig. S2e).

Activated HSCs can release a variety of chemokines and growth factors to recruit and activate leukocytes, among them CXCL1 (16), a mouse IL-8 homologue. In primary HSCs, we detected a dose-dependent increase of CXCL1 protein secretion with MPO, but not glucose oxidase (GOX, an H_2O_2 donor) stimulation (Fig. 5e). LPS also triggered CXCL1 secretion, although to approximately three-fold lower levels. RT-PCR confirmed an increase in *CXCL1*, but not *CXCL2*, in HSCs stimulated with MPO (Fig. 5e). Another cell capable of expressing CXCL1 is the hepatocyte (42). Stimulating primary mouse hepatocytes with GOX or MPO, however, did not result in an increase in CXCL1, while LPS showed modest efficiency to trigger hepatocyte CXCL1 secretion (Supplementary Fig. S2d). Applying these findings to NASH, we observed less CXCL1 protein and *CXCL1* mRNA in $MPO^{-/-}$ compared with WT mice (Fig. 5f).

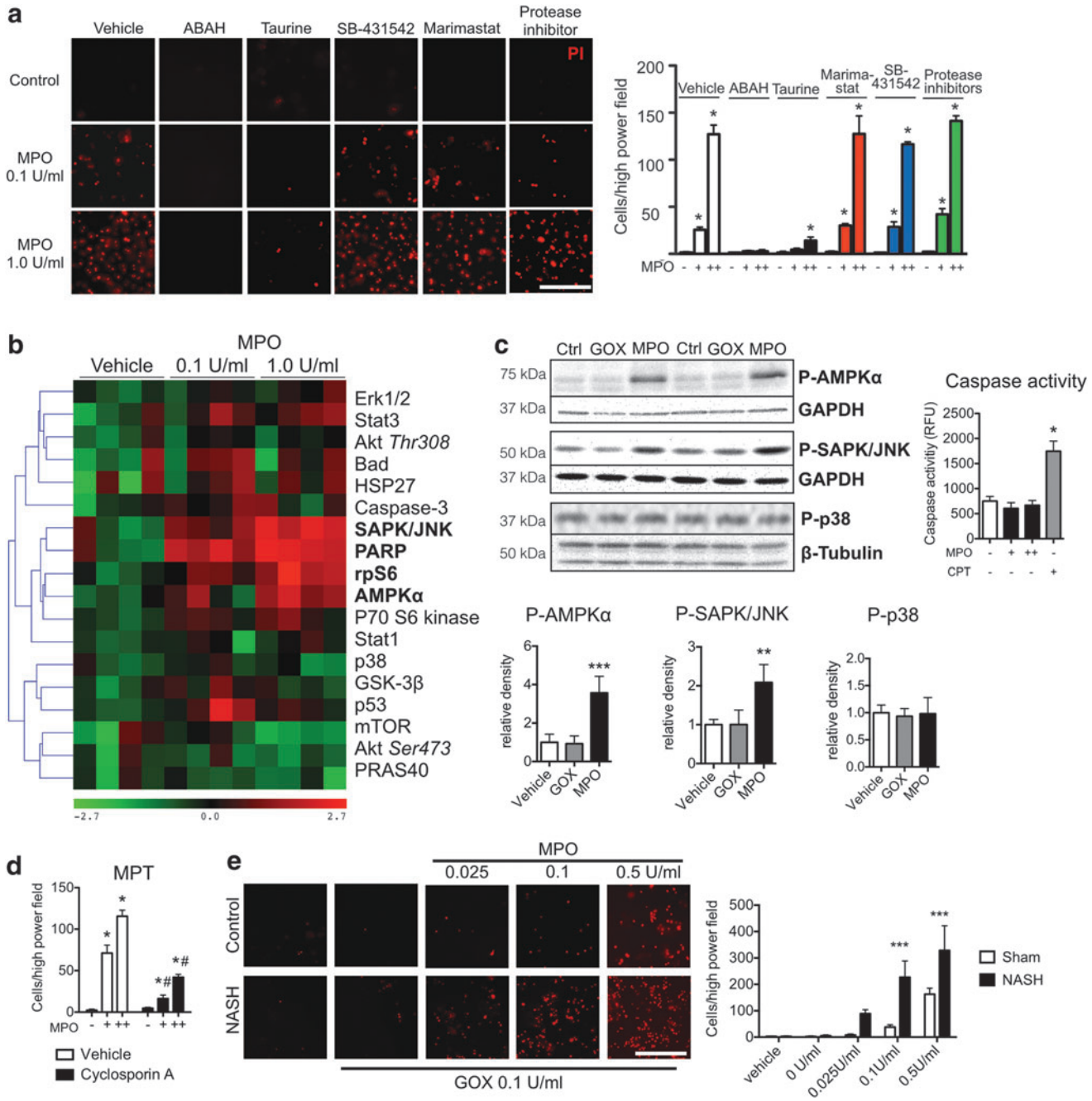

FIG. 4. MPO-derived oxidative stress causes hepatocyte injury *via* induction of mitochondrial permeability transition. **(a)** Cell death (propidium iodide, PI) in primary hepatocytes preincubated with ABAH, taurine, marimastat, SB-431542, or a protease inhibitor cocktail and incubated with MPO ($n=3$ per group, bar = 50 μm). **(b)** Heat map with hierarchical clustering of signaling pathways in primary hepatocytes stimulated with MPO. Molecules in *bold* are statistically significantly changed from baseline ($n=4$ per group). **(c)** Western blots of phosphorylated AMPK, SAPK/JNK, and p38, as well as caspase 3/7 activity in MPO- or vehicle-stimulated hepatocytes ($n=4$ per group). Camptothecin (CPT) was used as a positive control for the caspase assay. **(d)** Cell death in hepatocytes preincubated with the mitochondrial permeability transitioning pore inhibitor cyclosporine A ($n=4$ per group). **(e)** Cell death (propidium iodide, PI) in primary hepatocytes isolated from NASH or control mice and incubated with MPO ($n=4$ per group, bar = 50 μm). All data are mean ± SEM. For MPO, + = 0.1 U/ml, ++ = 1.0 U/ml. $^{*}p<0.05$, $^{**}p<0.01$, or $^{***}p<0.001$, $^{\#}p<0.05$ compared with vehicle. To see this illustration in color, the reader is referred to the web version of this article at www.liebertpub.com/ars

MPO activates TGF-β, and TGF-β inhibition ameliorates NASH

TGF-β has been identified as a crucial promoter of fibrogenesis (19). We tested whether MPO-induced oxidative stress could also activate TGF-β. *In vitro*, GOX-derived H_2O_2 alone did not activate latent TGF-β, but MPO-derived oxidative stress activated TGF-β in a dose-dependent way (Fig. 6a). In liver homogenates, we found significantly higher TGF-β levels in WT compared with $MPO^{-/-}$ NASH mice

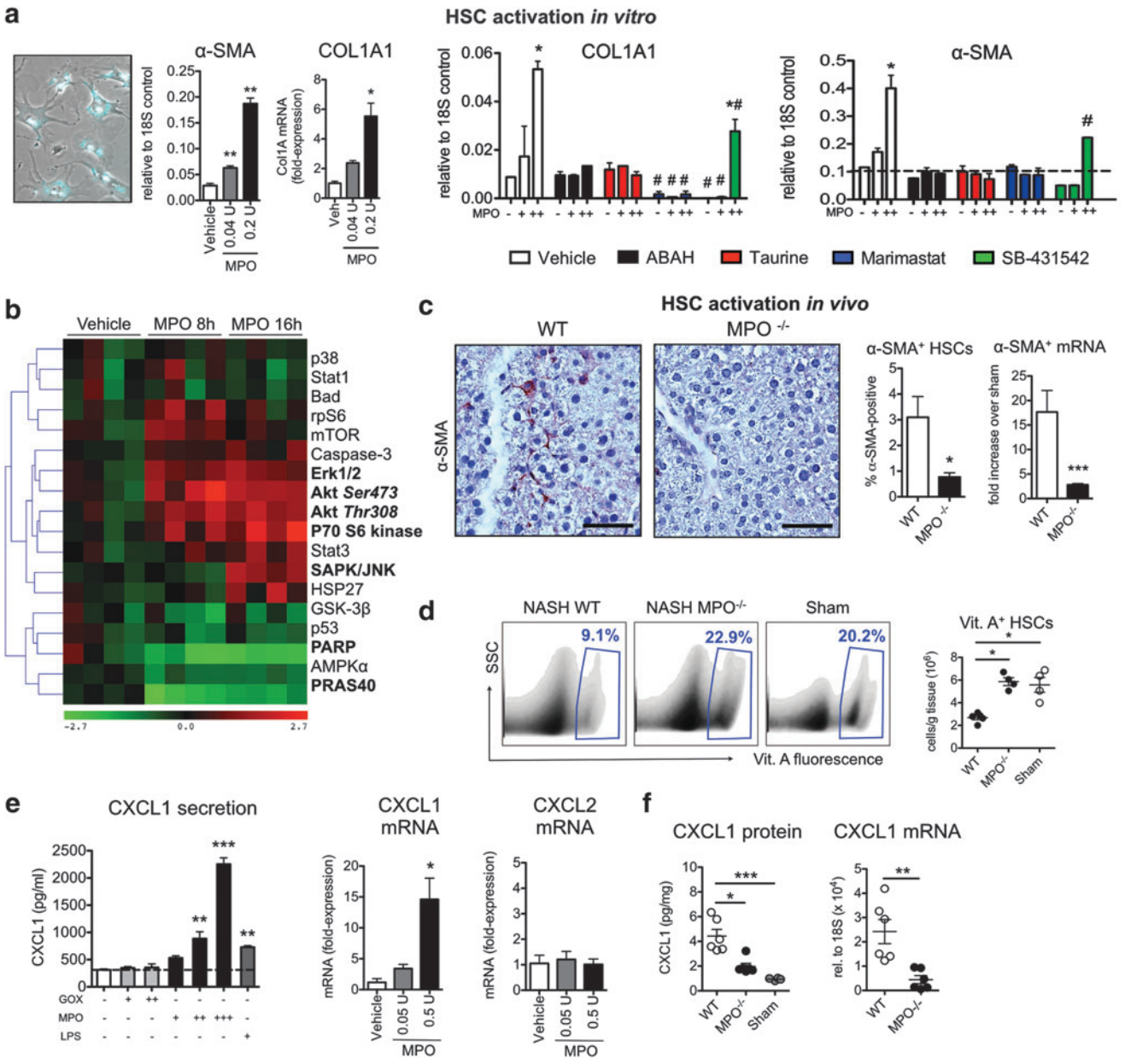

FIG. 5. MPO-derived oxidative stress activates hepatic stellate cells. (a) α-smooth muscle actin (α-*SMA*) and *COL1A1* expression of primary HSCs (bright-field and vitamin A fluorescence overlay, *left panel*) stimulated with MPO ($n = 3$–5 per group). Primary hepatic stellate cells (HSCs) were also preincubated with ABAH, taurine, marimastat, or SB-431542 and stimulated with MPO ($n = 3$ per group). **(b)** Heat map with hierarchical clustering of signaling pathways in primary HSCs stimulated with MPO. Molecules in *bold* are statistically significantly changed from baseline ($n = 4$ per group). **(c)** Immunohistochemistry for α-SMA (bar = 50 μm) and **(d)** flow cytometric analysis of vitamin A fluorescent quiescent HSCs ($n = 4$–5 per group). **(e)** CXCL1 protein secretion in primary HSCs ($n = 3$–4 per group). *CXCL1* and *CXCL2* mRNA in HSCs stimulated with MPO *in vitro*. **(f)** CXCL1 protein and mRNA levels in wild-type (WT) and MPO knockout ($MPO^{-/-}$) NASH mice, as well as sham mice ($n = 6$ per group). All data are mean ± SEM. + = 0.05 U/ml, ++ = 0.5 U/ml, $^{*}p < 0.05$, $^{**}p < 0.01$, $^{***}p < 0.001$, $^{\#}p < 0.05$ compared to vehicle. To see this illustration in color, the reader is referred to the web version of this article at www.liebertpub.com/ars

(Fig. 6b). These findings indicate that MPO contributes to TGF-β activation. To investigate the effect of TGF-β signaling inhibition with SB-431542, which inhibited MPO-mediated HSC activation *in vitro* (Fig. 5a), we treated NASH mice with SB-431542 for 4 weeks. On histology, SB-431542-treated mice demonstrated reduced steatosis and fibrosis similar to MPO-KO mice (Fig. 6c, d), and the NAS was significantly reduced (Fig. 6c, d).

Myeloid cell recruitment and cytokine secretion remain unaffected by MPO deficiency

To investigate the role of MPO in myeloid cell recruitment and secretion of TNF and TGF-β, we performed flow cytometry (Fig. 7a). We did not find a difference in neutrophils, monocytes, or Kupffer cells between the WT and $MPO^{-/-}$ mice, whereas all of these cell subsets were increased

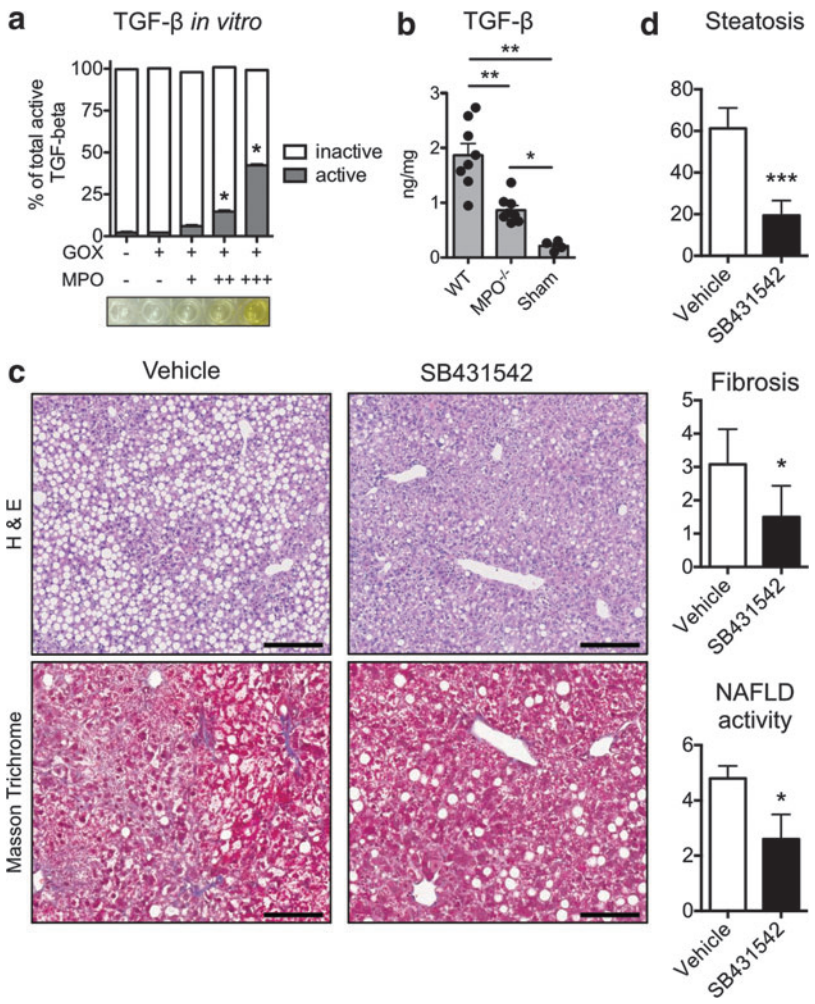

FIG. 6. MPO activates TGF-β, and TGF-β signaling inhibition ameliorates steatosis and fibrosis in NASH. (a) Activation of TGF-β *in vitro*. TGF-β was incubated with glucose oxidase (GOX) and MPO ($n=3$ per group). $+=0.01$ U/ml. $++=0.1$ U. $+++=1$ U/ml. **(b)** TGF-β in wild-type (WT) and MPO knockout ($MPO^{-/-}$) mice with NASH and sham mice ($n=6$ per group). **(c)** Hematoxylin and eosin (H&E, bars = 100 μm) and Masson's trichrome (collagen in *blue*, bars = 500 μm) stains of liver sections from NASH mice treated with the TGF-β signaling inhibitor SB-431542 or vehicle for 4 weeks. **(d)** Quantification of steatosis, fibrosis, and NAFLD activity. All data are mean ± SEM. $+=0.05$ U/ml, $++=0.5$ U/ml, $*p<0.05$, $**p<0.01$, $***p<0.001$. To see this illustration in color, the reader is referred to the web version of this article at www.liebertpub.com/ars

compared with those from sham mice. Next, we evaluated TNF secretion by Ly-$6C^{high}$ monocytes and TGF-β secretion by Kupffer cells, both of which contribute to liver fibrosis (51), but did not find a significant difference (Fig. 7b, d). Similarly, we did not detect a difference in total liver TNF levels (Fig. 7c).

Discussion

Our study establishes three previously undescribed functions of MPO: (i) MPO potentiates oxidative stress to cause hepatocyte death, a hallmark of progression in NAFLD; (ii) MPO activates HSCs, the main source of collagen in the liver, to upregulate collagen and secrete CXCL1; and (iii) MPO activates TGF-β, a crucial profibrotic cytokine, and TGF-β inhibition resulted in decreased steatosis and fibrosis in mice with NASH (Fig. 8). Furthermore, because $MPO^{-/-}$ mice induced with NASH showed improved fibrosis and attenuated hepatocyte injury, our results further suggest that MPO could be a promising therapeutic target in NAFLD and liver fibrosis.

Besides leukocytes, hepatocytes (8) and HSCs (5) are capable of generating oxidative stress that can be catalyzed into more toxic hypochlorous acid, chloramines, or reactive nitrogen species by MPO. While the precursors (*e.g.*, O_2^-, H_2O_2) are short-lived *in vivo*, these MPO-derived ROS have longer half-lives and can penetrate the extracellular fluid to exert their toxic effects at a distance (24). Indeed, our data indicate that MPO triggers hepatocyte death *in vitro* and *in vivo* and transforms the less damaging H_2O_2 into more damaging products like HOCl. Our finding of colocalization of MPO with injured liver cells further corroborates this.

While MPO-derived ROS have been implicated in hepatocyte injury (20), their importance to NASH and molecular mechanism had not been investigated. We found that MPO-derived HOCl triggers hepatocyte death independent of MMPs, proteases, and TGF-β. MPO-induced hepatocyte death was increased in hepatocytes isolated from NASH mice compared with control mice, suggesting increased susceptibility to MPO, in line with reports that antioxidative capacity is reduced in NASH (39). Furthermore, we detected increased phosphorylation of JNK, PARP, rpS6, and AMPK in hepatocytes stimulated with MPO, while no increase in caspase activity was observed. Phosphorylation of JNK results in mitochondrial oxidative/nitrosative stress (48) and has been shown to promote hepatocyte death (47). PARP can be activated by oxidative stress (10) and PARP activation leads to depletion of ATP and NAD^+ (48). The combination of these events therefore likely induces MPT and necrosis. This is consistent with our finding that cyclosporine A, an inhibitor of the MPT, reduced MPO-induced hepatocyte death. Without MPO, the liver is capable of ameliorating the effects of ROS caused by the MCD diet.

Activated HSCs are the main collagen-producing cells in the liver (16). Although hepatocytes, endothelial cells, and Kupffer cells have been shown to interact with HSCs, we

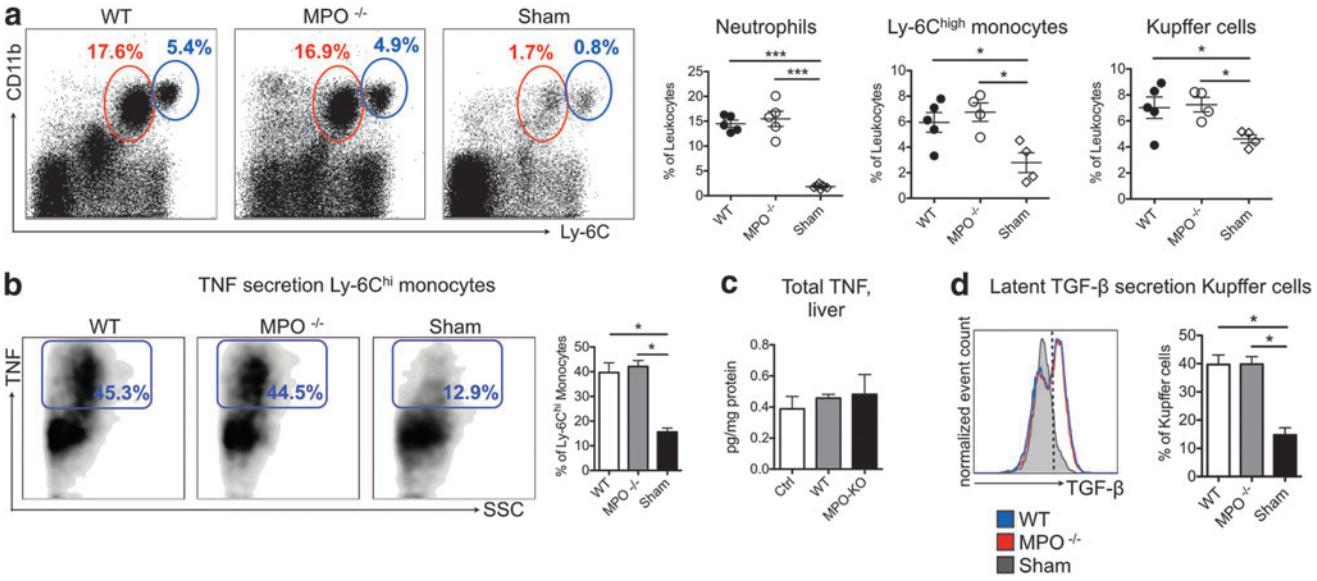

FIG. 7. Myeloid cell subsets and cytokine expression are similar in MPO knockout and wild-type mice with NASH. **(a)** Liver myeloid cell populations in wild-type (WT) and MPO knockout ($MPO^{-/-}$) with NASH and sham mice. Representative analysis of neutrophils (*red gate*) and Ly-$6C^{high}$ monocytes (*blue gate*) is shown, and relative numbers of neutrophils, monocytes, and Kupffer cells are presented ($n = 4$–5 per group). **(b)** TNF secretion of Ly-$6C^{high}$ monocytes ($n = 4$–5 per group). **(c)** Total liver TNF levels as determined by ELISA ($n = 5$ per group). **(d)** TGF-β secretion of Kupffer cells ($n = 4$–5 per group). All data are mean ± SEM. $^{*}p < 0.05$, $^{***}p < 0.001$. To see this illustration in color, the reader is referred to the web version of this article at www.liebertpub.com/ars

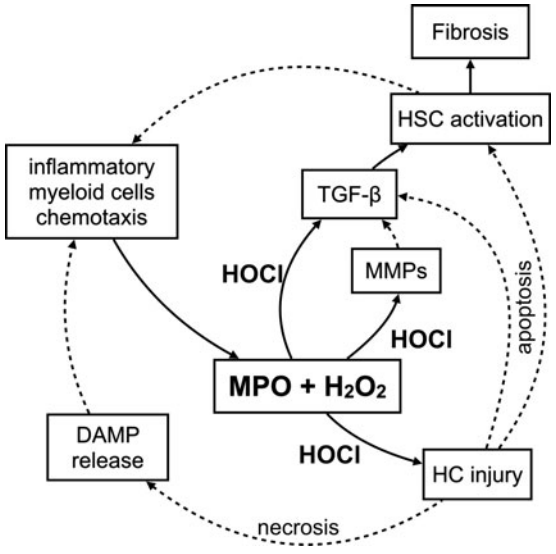

FIG. 8. Pathophysiology of NASH relevant to MPO. MPO catalyzes the formation of hypochlorous acid (HOCl) from hydrogen peroxide (H_2O_2). This induces hepatocyte (HC) injury. HS apoptosis leads to TGF-β secretion and HSC activation. HOCl also activates TGF-β and matrix metalloproteinases (MMPs), resulting in hepatic stellate cell (HSC) activation. Activated HSCs deposit collagen and thus contribute to fibrosis. Activated HSCs secrete chemokines to attract inflammatory myeloid cells CXCL1. HC necrosis releases damage-associated molecular pattern molecules (DAMPs), among other factors, which also recruit inflammatory myeloid cells to the site of injury. *Solid lines* represent findings from the present article, and *dashed lines* are included to link these findings to established knowledge.

report here a new link between neutrophil and monocyte-derived MPO and HSCs. HSCs have been shown to express NADPH oxidase (5) and thus generate O_2^-, which in turn is converted to H_2O_2, and MPO can then catalyze the formation of HOCl. We showed that MPO induces upregulation of α-SMA, a well-established marker of HSC activation (16), as well as collagen *in vitro*. In neutrophil-HSC coculture, activated neutrophils were capable of activating HSCs, as demonstrated by upregulation of α-SMA and collagen, and this effect could be inhibited by MPO inhibition. *In vivo*, reduced α-SMA protein and mRNA expression, decreased expression of collagen, and increased numbers of vitamin A-containing quiescent HSCs were observed in $MPO^{-/-}$ mice compared with WT with NASH.

HSC activation is a complex process involving multiple signaling cascades. Our experiments demonstrate that MPO-derived HOCl activation of HSCs is MMP dependent and partially TGF-β dependent. This is consistent with prior studies suggesting that MMP activity is crucial for HSC activation by different stimuli (18, 33). Furthermore, several key profibrotic signaling nodes (JNK/ERK as well PI3K-Akt-S70S6K) are phosphorylated upon stimulation of HSCs with MPO. Relevant to NASH, in previous studies, activation of JNK, ERK, or JNK led to HSC activation (29, 37, 38), and JNK inhibition reduced liver fibrosis in mice after BDL or CCl4 treatment (26).

JNK activation can be induced by oxidative stress, and interestingly activated JNK itself can induce mitochondrial ROS production (52). Thus, MPO may activate HSCs directly *via* its product HOCl or indirectly by inducing mitochondrial ROS/RNS production *via* JNK. While we detected a robust increase of CXCL1 in MPO-activated HSCs, we did not find a difference in myeloid cell recruitment. This was

surprising at first, but may be explained by redundancy in the chemokine system as well as by very localized effects of CXCL1 around HSCs in the perisinusoidal space, where CXCL1 does not reach myeloid cells that circulate in blood vessels.

It has been reported that hepatocyte apoptosis triggers HSC activation (55) likely *via* TGF-β, and deficient TGF-β signaling in hepatocytes resulted in decreased steatosis, fibrosis, and inflammation (56). While our findings show that MPO can by itself induce HSC activation, it is likely that *in vivo*, both MPO and apoptotic hepatocytes contribute to HSC activation, especially when considering that MPO directly causes hepatocyte injury and activates TGF-β.

TGF-β is one of the most important profibrotic cytokines (19). Oxidative stress, acidic conditions, and MMPs have been shown to activate TGF-β. MPO causes oxidative stress, catalyzes the production of hypochlorous acid, and activates and increases MMPs, which make it an ideal candidate to modulate TGF-β activity. Indeed, in our experiments, MPO-derived products (*e.g.*, HOCl)—but not H_2O_2—directly activated TGF-β *in vitro* and, more importantly, contributed to TGF-β activity *in vivo*. Both TGF-β activation and induction of hepatocyte death may explain the surprising finding that $MPO^{-/-}$ NASH mice had decreased steatosis. Absent TGF-β signaling in hepatocytes results in decreased steatosis in mice fed a choline-deficient diet (56). Similarly, TGF-β inhibition by SB431542 resulted in decreased steatosis and fibrosis in our experiments. These findings link MPO to steatosis *via* induction of hepatocyte death and activation of TGF-β.

Our findings could translate into both diagnostic and therapeutic advances in NAFLD in humans. Diagnostically, MPO could be used as a biomarker to distinguish NASH from steatosis and to evaluate disease activity and risk of progression. This could be accomplished with a molecular MR imaging probe specific for MPO enzymatic activity (9). Alternatively, recent advances in optical imaging could allow for bioluminescence imaging of MPO activity (57). These approaches would allow for longitudinal and noninvasive monitoring of MPO activity *in vivo* and circumvent sampling error, a well-known shortcoming of liver biopsies (36).

Therapeutically, our results strongly suggest a potential for MPO as a treatment target in NASH. While there are several MPO inhibitors for research use, there is currently no clinically available drug that specifically inhibits MPO. However, an MPO inhibitor named AZD3241 has recently completed a phase IIa trial, and several preclinical candidates are under development (15, 53). An additional benefit of targeting MPO is that side effects are likely to be minimal given that individuals with hereditary MPO deficiency are mostly asymptomatic (27).

Materials and Methods

Induction of NASH and animal protocol

The protocol for animal experiments was approved by the institutional animal care committee (IACUC). Eight- to twelve-week-old female $MPO^{-/-}$ ($n = 34$; Jackson Laboratories) and C57Bl/6J WT mice ($n = 54$; Jackson Laboratories) were fed a diet deficient in methionine and choline (MCD diet; Teklad Harlan) for 4 weeks to induce NASH (54) or a control diet (diet composition, Supplementary Table S1) for the same period of time (sham). For treatment experiments, mice were treated with 10 mg/kg SB-431542 (Cayman Chemicals) intraperitoneally daily from day 0 for 4 weeks.

MPO ELISA and antibody capture activity assay

MPO activity and protein were measured as described previously (34). Briefly, we homogenized liver tissue in cetyltrimethylammonium bromide buffer, and after sonication, supernatants were used for MPO assays. To specifically capture MPO, aliquots were incubated on MPO ELISA plates (Hycult). MPO activity of antibody-captured MPO was assessed with 10-acetyl-3,7-dihydroxyphenoxazine (ADHP; AAT Bioquest) and a Safire 2 microplate reader (Tecan) at EX535/EM590 (34). After data acquisition, sandwich MPO ELISA was performed according to the manufacturer's protocol.

Extracellular protein extraction. For MPO to cause effects outside of myeloid cells, it must be secreted into the extracellular space. We therefore used a recently validated method to extract liver extracellular fluid (34). Briefly, livers were incubated for 2 h in extraction buffer (0.32 *M* sucrose, 1 m*M* $CaCl_2$, 10 U/ml heparin), followed by acetone protein precipitation. This was performed to concentrate the very diluted extracellular fraction. MPO activity was assessed on extracellular fractions using the same antibody capture assay as described above. To determine specificity of our activity assay, we also utilized $MPO^{-/-}$ mice.

Biochemical and immunological assays

Hydroxyproline content was measured with a colorimetric assay after hydrolyzing collagen with HCl as per the manufacturer's instructions (BioVision).

CXCL1 in conditioned culture medium and samples from WT and $MPO^{-/-}$ NASH mice were measured with a bead-based flow cytometry immunoassay (CXCL1 FlowCytomix; eBioscience) as per the manufacturer's instructions.

Active TGF-β was detected with ELISA (R&D Systems) as per the manufacturer's instructions. Latent TGF-β was gathered from HT-1080 cells (ATCC CCL-121, human fibrosarcoma). Briefly, HT-1080 cells were washed and incubated with serum-free MEM with protease inhibitors (Roche) for 36 h, and conditioned medium was harvested. Increasing concentrations of purified human MPO (Lee Biosolutions) and GOX were added as a source of H_2O_2 and incubated for 2 h. One part of each sample was then activated with 1 *M* HCl and neutralized with 1.2 *M* NaOH to measure the total amount of TGF-β, the other one was left inactivated to measure active TGF-β. For *in vivo* assessment of TGF-β, half of each sample was treated with HCl (total amount of TGF-β) and the other half was left untreated (active TGF-β). Active and inactive TGF-β were then measured with ELISA and reported as ng per mg BCA protein.

Caspase 3/7 activity was measured with the fluorogenic substrate (Z-Asp-Glu-Val-Asp)2-R110 as per the manufacturer's instructions (Promega). Briefly, hepatocytes were isolated and incubated with GOX and MPO as described above. Camptothecin at a concentration of 5 μM was used as a positive control. Then, cells were incubated with caspase 3/7 reagent for 12 h at RT protected from light, and fluorescence was measured with a Safire 2 microplate reader (Tecan) at an excitation wavelength of 499 nm and an emission wavelength of 521 nm.

To evaluate the effect of ABAH, taurine, marimastat, SB431542, and cyclosporine A on HOCl production, we utilized luminol (46) (Sigma). Briefly, 10 μl of the sample was combined with 40 μl of 250 μM luminol in PBS and 50 μl of 100 μM H_2O_2 in PBS. Bioluminescence was then immediately measured with a Safire 2 microplate reader (Tecan).

Liver homogenates from NASH and control mice were also assayed for TNF content by ELISA (R&D Systems) according to the manufacturer's instructions. Results were normalized to BCA protein content of liver protein extracts.

Serum samples and homogenates from visceral fat tissue from NASH and control mice were assayed for adiponectin content by ELISA (R&D Systems) according to the manufacturer's instructions. Serum samples and liver homogenates were assayed for endotoxin levels using the LAL chromogenic endotoxin kit (Thermo Scientific) according to the manufacturer's instructions.

Liver leukocyte isolation. Mice were anesthetized using 1–3% isoflurane (Forane, Baxter), transcardially perfused with 20 ml ice-cold phosphate-buffered saline (PBS), and liver leukocytes were isolated using centrifugation at 50 *g* to remove parenchymal cells, followed by centrifugation over a discontinuous (35%) Percoll (GE Healthcare) gradient (7). The enriched liver leukocyte fraction was then washed in staining buffer (Dulbecco's phosphate-buffered saline [DPBS], 1% fetal bovine serum [FBS], 0.5% bovine serum albumin [BSA]), and used for subsequent flow cytometric analysis.

Neutrophil activation. First, we determined conditions of secretion for MPO and elastase from neutrophils. Neutrophils were isolated from bone marrow as follows: tibias and fibulas were harvested, epiphyses cut, and bone marrow cells flushed out with HBSS containing 1% FBS and 0.5% BSA. Cells were filtered through a 40-μm cell strainer (BD Bioscience), and RBCs were lysed with RBC lysis buffer (BioLegend). Neutrophils were then enriched over a 62% Percoll gradient by centrifugation at 1000 g for 30 min at RT. The pellet containing the enriched neutrophils was resuspended in complete DMEM, counted, and used for activation experiments at a concentration of 2×10^6 cells per ml.

Cells were stimulated with 500 or 2000 ng/ml ionomycin. MPO activity was measured as described above. Neutrophil respiratory burst formation was assessed by superoxide production measurements using dihydroethidium (DHE, Cayman chemicals) (58). Briefly, DHE at 10 μM was added to the cells for 20 min, followed by detection of fluorescence (ex: 480 nm, em: 567 nm) on a Safire 2 microplate reader (Tecan) at EX480/EM567.

Neutrophil-HSC coculture

Neutrophils and HSCs were isolated as described above. On day 2, neutrophils were stimulated with fMLP and 0.5×10^6 cells added to each well with HSCs. At 2 and 6 h, the medium was removed and fresh activated neutrophils were added. Supernatant was harvested for MPO activity assay and mRNA isolated from cells as described above.

Nonparenchymal cell, HSC, and hepatocyte isolation

For isolation of hepatocytes, 6- to 12-week-old female C57Bl/6J ($n = 7$) mice were used, while for isolation of nonparenchymal cells (NPCs)/HSCs, either 8- to 20-week old female C57BL/6J ($n = 13$) or BALB/c mice ($n = 15$; Jackson Laboratories) were used. Mice were anesthetized as above and the inferior vena cava was cannulated. The superior vena cava was clamped and the portal vein was cut. For NPC extraction, the liver was perfused with 0.05% collagenase (Sigma) and 1 U/ml dispase (Roche) and liver tissue further digested with collagenase for 30 min at 37°C. Parenchymal cells were removed from the cell suspension by centrifugation at 50 *g* thrice. For HSC isolation, livers were first perfused with 1 mg/ml pronase (Sigma), then 0.5 mg/ml collagenase (Sigma), and liver tissue further digested in 0.5 mg/ml collagenase and 0.5 mg/ml pronase for 20 min at 37°C (30). HSCs were then enriched over a 9% Optiprep (Axis Shield) gradient as described previously (11). For isolation of hepatocytes, livers were perfused with 100 CDU/ml collagenase (C5138; Sigma), and hepatocytes were purified by centrifugation at 50 *g* thrice.

HSC and hepatocyte activation. Enriched HSCs were resuspended in complete DMEM (10% FBS) and plated on 48-well plates at 1×10^5 cells/ml. Hepatocytes were plated on 24-well plates at 2×10^5 cells/ml. For HSCs, the medium was changed at 2 h, and at 24 h, the medium was changed to DMEM with 0.5% FBS. For hepatocytes, the medium was changed at 1 h, and then the medium was changed to DMEM with 0% FBS at 4–6 h. HSCs or hepatocytes were then incubated for 4–24 h with LPS (Sigma; 100 ng/ml), purified MPO (0.005–1 U/ml), or glucose oxidase (GOX; Affymetrix; 0.005–0.05 U/ml), and conditioned medium was harvested for CXCL1 and neutrophil activation experiments. Cells were also harvested for measuring GFAP expression with flow cytometry and for RT-PCR. For some experiments, HSCs or hepatocytes were also preincubated with 100 nM marimastat (Tocris), 1 μM SB-431542 (Tocris), 5 mM taurine (Sigma), 200 μM ABAH (Sigma), 10 μM cyclosporine A (Sigma), or 1 tab/10 ml protease inhibitor (cOmplete mini; Roche). To assess hepatocyte viability, propidium iodide (PI; Sigma) at a concentration of 5 μg/ml was added, and 30 min later, cells were washed in HBSS and analyzed for PI uptake under an inverted microscope (Nikon E2000, EX562/40, EM624/40).

Flow cytometry

All antibodies were purchased from BD Bioscience, unless otherwise indicated (Supplementary Table S2). For intracellular staining of MPO, cells were fixed and permeabilized (Cytofix/Cytoperm; BD Bioscience), followed by staining for MPO. For evaluation of tumor necrosis factor (TNF) and TGF-β expression, cells were stimulated with PMA (50 ng/ml; Sigma) and ionomycin (250 ng/ml; Sigma) in the presence of monensin and brefeldin A at recommended concentrations (BD Bioscience), fixed/permeabilized, and stained with anti-TNF and anti-TGF-β. Vitamin A fluorescence in HSCs was detected through excitation with a 355 nm UV laser and detection with a 450/50 filter (32). Viable cells were determined by adding 1 μg/ml 4',6-diamidino-2-phenylindole (DAPI; Invitrogen) to the cell suspension immediately before analysis and excluding the DAPI-positive cells. Cells were counted with a hematocytometer, and the cell numbers of different cell populations were calculated as

total cells multiplied by the percentage within the respective cell population gate. Data were acquired on an LSRII (BD Bioscience) and analyzed with FlowJo 887 (Tree Star, Inc.). Neutrophils were identified as $CD11b^{high}$ (B220/CD90/CD49b/NK1.1/Ly-6G)^{high} $F4/80^{low}$ Ly-$6C^{int}$. Monocytes were identified as $CD11b^{high}$ (B220/CD90/CD49b/NK1.1/Ly-6G)^{low} $F4/80^{low}$ $CD115^{high}$ and divided into Ly-$6C^{high}$ and Ly-$6C^{low}$ monocyte subsets based on Ly-6C and CD11c expression. Kupffer cells were identified as (B220/CD90/CD49b/NK1.1/Ly-6G)^{low} $F4/80^{high}$ $CD11b^{int}$ Ly-$6C^{low}$. Quiescent HSCs were identified as (B220/CD90/CD49b/NK1.1/Ly-6G/CD11b/Ly6C)^{low} vitamin A^{high}. Activated HSCs were identified as (B220/CD90/CD49b/NK1.1/Ly-6G/CD11b/Ly6C)^{low} $GFAP^{high}$.

Quantitative real-time PCR

Liver specimens were flash-frozen in liquid NO2 and stored at −80°C, then homogenized using a TissueRuptor mechanical homogenizer (Qiagen) in RNeasy lysis buffer (RLT; Qiagen) supplemented with 1% 2-mercaptoethanol (2-ME; Sigma). For experiments involving purified HSCs, approximately 50,000 cells were resuspended into RLT with 1% 2-ME. mRNA was then isolated with the RNeasy RNA isolation kit (Qiagen) as per the manufacturer's instructions. cDNA was generated using the high-capacity reverse transcription kit (Applied Biosystems). Expression of mRNAs was determined using gene-specific TaqMan probes (Supplementary Table S3). Reactions were run on an ABI 7500 Fast Real-Time PCR machine (Applied Biosystems) in triplicate 10 μl reactions using standard machine settings. Expression data were normalized using 18s rRNA endogenous control and relative expression values were calculated.

Intracellular signaling array

A slide-based array (Cell Signaling Technologies) using the sandwich ELISA principle, where target-specific capture antibodies are spotted in duplicates onto nitrocellulose-coated glass slides, was used as per the manufacturer's instructions. After incubation with a secondary biotinylated antibody cocktail and Alexa Fluor 647 streptavidin conjugate, the slides were captured with a microarray scanner (GenePix 4000b; Molecular Devices) and spot intensities quantified using the protein array analyzer plugin for ImageJ. Analysis of the resulting data was then performed using Excel (Microsoft) and statistically analyzed with MeV (44). Heat maps with hierarchical clustering were created using MeV.

Western blotting of phosphorylated signaling proteins

Protein concentration of hepatocyte lysates was measured with the BCA Protein Assay Kit (Thermo Scientific) according to the manufacturer's instructions. For SDS-PAGE, samples were diluted 1:1 in 2×Laemmli sample buffer (Bio-Rad Laboratories, Inc.) supplemented with 5% v/v 2-mercaptoethanol (Sigma) and heated to 95°C for 5 min; 15–30 μg of protein was separated on hand-cast 10- or 15-well 12% polyacrylamide gels. After SDS-PAGE, proteins were transferred by Western blotting onto PVDF membranes, and membranes were blocked with 5% BSA in TBST for 1 h at room temperature. Membranes were then incubated with the primary rabbit antibody (Phospho-SAPK/JNK, #9251; Phospho-AMPKα, #2531; Phospho-p38 MAPK, #9215; Phospho-Stat1, #7649; Stat1, #9172, all from Cell Signaling Technology) at a dilution of 1:1000 overnight at 4°C. On the following day, membranes were washed and incubated with the secondary HRP-linked anti-rabbit IgG antibody (#7074; Cell Signaling Technology®) at a dilution of 1:1000 for 1 h at room temperature, followed by incubation with substrate solution (Thermo Scientific), and imaged on an AlphaImager 2200 (Alpha Innotech) imaging system. Images were quantified using ImageJ software. Membranes were then stripped, blocked again, and incubated with the loading control (anti-GAPDH antibody ab9485; or anti-beta Tubulin antibody ab6046, both from Abcam) at a dilution of 1:1000 for 1 h at room temperature, followed by secondary antibody, substrate, and image acquisition as above.

Immunohistochemistry and immunofluorescence. Livers were fixed in 4% paraformaldehyde in PBS, paraffin embedded, and cut on a microtome to 7 μm thickness. The paraffin-embedded sections were deparaffinized and rehydrated. After antigen retrieval, tissue sections were incubated in 1% hydrogen peroxide solution for 10 min and blocked with 4% normal rabbit or goat serum in PBS. Sections were then incubated with purified anti-mouse Ly-6G (1A8; BioLegend), MPO (Ab-1; Thermo Fisher Scientific), or anti-alpha smooth muscle actin (Abcam) overnight at 4°C. Biotinylated secondary antibodies (Vector Laboratories, Inc.), followed by VECTASTAIN ABC reagent (Vector Laboratories, Inc.), were applied to tissue sections. Red reaction products were produced by 3-amino-9-ethylcarbazole (Dako). Trichrome (Masson's) staining was performed using a trichrome stain kit (Sigma). Hematoxylin and eosin (H&E) staining was performed for overall morphology. The images of all the slides were captured and digitized automatically at a magnification of 40×(NanoZoomer 2.0RS; Hamamatsu).

Immunofluorescence staining. For immunofluorescence staining, paraffin-embedded sections were prepared as above. Alexa Fluor 594 chicken anti-rabbit IgG antibody and Alexa Fluor 488 goat anti-rat IgG antibody (both from Invitrogen) were used as secondary antibodies. The fluorescence images were captured using a BX63 (Olympus) equipped with Neo sCMOS (ANDOR Technology)—TXRED: EX562/40, EM624/40, and DM593 for MPO and FITC: EX472/30, EM520/35, and DM495 for Ly-6G.

For assessment of hepatocyte injury, mice were injected intravenously with Sytox Red (Invitrogen; 1:250 in 100 μl normal saline) and livers were harvested 15 min later. Livers were then fixed in 4% paraformaldehyde for 12 h, incubated in 30% sucrose in PBS overnight, frozen in OCT (Fisher Scientific), and cut into 6-μm sections on a cryotome. At least three sections per mouse were then evaluated for Sytox Red-positive cells. In addition, hepatocytes were isolated as above and Sytox Red fluorescence was excited with a 633 nm laser and detected with a 660/20 filter with flow cytometry.

Quantification of tissue sections was performed by either manually counting positive cells (Ly-6G, MPO, and ballooning hepatocytes) by two blinded reviewers (A.M. and B.P.) or by unbiased measurements of the positively stained area using the color threshold function in ImageJ (NIH) (fibrosis, α-SMA). For Sytox Red, positively stained cells were also quantified by applying a color threshold in ImageJ,

followed by encircling positive cells using the outer glow effect in Photoshop CS5 (Adobe). This was done to allow visualization of positive cells at low magnification for whole liver lobes and verified in multiple sections for reliability and accuracy.

Oil Red O assay

To quantify the liver lipid content, we incubated fresh liver tissue in 10% PFA in PBS for 4 h at RT, then cut the tissue in 1×1 mm pieces, and washed it twice with dH2O. We then added 500 μl of 0.3% Oil Red O in 60% isopropanol, incubated it for 1 h at 70°C, and washed it with dH2O five times. We extracted Oil Red O from the tissue with 300 μl of 100% isopropanol for 10 min at 70°C, and absorbance at 520 nm was measured with a Safire 2 microplate reader (Tecan).

NAFLD activity score. The NAS was evaluated by two independent blinded reviewers (A.M. and B.P.) as described before (25). Briefly, two sections per animal were evaluated for steatosis (grade and location), fibrosis and inflammation (fibrosis stage and lobular/periportal inflammation), and liver cell injury (ballooning and megamitochondria) on H&E and Masson's trichrome staining.

Statistical analysis

Statistical analysis of the data was performed using GraphPad Prism software (GraphPad Software, Inc.). Results are expressed as mean ± SEM. Statistical tests included Student's *t*-test using Welch's correction for unequal variances and Mann–Whitney *U* test for non-normal distributed data. Three or more groups were compared with one-way ANOVA, followed by the Bonferroni post-test. For categorical data, Fisher's exact test was utilized. Signaling array data were compared with MeV using significance analysis of microarrays (44). A *p*-value equal or less than 0.05 was considered statistically significant.

Financial Support

B.P. has received a fellowship from the Ernst Schering Foundation in Berlin, Germany, and a grant from the National Natural Science Foundation, Beijing, China. This study was supported, in part, by the NIH (R01-NS070835 and R01-NS072167 to J.W.C.).

Author's Contributions

Study concept and design were done by B.P. and J.W.C.; acquisition of data by B.P., M.A., Y.I., and M.W.Z.; analysis and interpretation of data by B.P., J.W.C., S.S., and J.L.; drafting of the manuscript by B.P. and J.W.C.; and revision of the manuscript for important intellectual content by B.P., M.A., Y.I., M.W.Z., S.S., J.J., and J.W.C.

Author Disclosure Statement

No competing financial interests exist.

References

1. Adams LA and Angulo P. Recent concepts in non-alcoholic fatty liver disease. *Diabet Med* 22: 1129–1133, 2005.
2. Alano CC, Ying W, and Swanson RA. Poly(ADP-ribose) polymerase-1-mediated cell death in astrocytes requires NAD+ depletion and mitochondrial permeability transition. *J Biol Chem* 279: 18895–18902, 2004.
3. Amanzada A, Malik IA, Nischwitz M, Sultan S, Naz N, and Ramadori G. Myeloperoxidase and elastase are only expressed by neutrophils in normal and in inflamed liver. *Histochem Cell Biol* 135: 305–315, 2011.
4. Bachem MG, Meyer D, Melchior R, Sell KM, and Gressner AM. Activation of rat liver perisinusoidal lipocytes by transforming growth factors derived from myofibroblastlike cells. A potential mechanism of self perpetuation in liver fibrogenesis. *J Clin Invest* 89: 19–27, 1992.
5. Bataller R, Schwabe RF, Choi YH, Yang L, Paik YH, Lindquist J, Qian T, Schoonhoven R, Hagedorn CH, Lemasters JJ, and Brenner DA. NADPH oxidase signal transduces angiotensin II in hepatic stellate cells and is critical in hepatic fibrosis. *J Clin Invest* 112: 1383–1394, 2003.
6. Bellentani S and Marino M. Epidemiology and natural history of non-alcoholic fatty liver disease (NAFLD). *Ann Hepatol* 8 Suppl 1: S4–S8, 2009.
7. Blom KG, Qazi MR, Matos JB, Nelson BD, DePierre JW, and Abedi-Valugerdi M. Isolation of murine intrahepatic immune cells employing a modified procedure for mechanical disruption and functional characterization of the B, T and natural killer T cells obtained. *Clin Exp Immunol* 155: 320–329, 2009.
8. Carmona-Cuenca I, Herrera B, Ventura JJ, Roncero C, Fernandez M, and Fabregat I. EGF blocks NADPH oxidase activation by TGF-beta in fetal rat hepatocytes, impairing oxidative stress, and cell death. *J Cell Physiol* 207: 322–330, 2006.
9. Chen JW, Querol Sans M, Bogdanov A, Jr., and Weissleder R. Imaging of myeloperoxidase in mice by using novel amplifiable paramagnetic substrates. *Radiology* 240: 473–481, 2006.
10. Chen M, Zsengeller Z, Xiao CY, and Szabo C. Mitochondrial-to-nuclear translocation of apoptosis-inducing factor in cardiac myocytes during oxidant stress: potential role of poly(ADP-ribose) polymerase-1. *Cardiovasc Res* 63: 682–688, 2004.
11. Connolly MK, Bedrosian AS, Mallen-St Clair J, Mitchell AP, Ibrahim J, Stroud A, Pachter HL, Bar-Sagi D, Frey AB, and Miller G. In liver fibrosis, dendritic cells govern hepatic inflammation in mice via TNF-alpha. *J Clin Invest* 119: 3213–3225, 2009.
12. Duffield JS, Forbes SJ, Constandinou CM, Clay S, Partolina M, Vuthoori S, Wu S, Lang R, and Iredale JP. Selective depletion of macrophages reveals distinct, opposing roles during liver injury and repair. *J Clin Invest* 115: 56–65, 2005.
13. Ekstedt M, Franzen LE, Mathiesen UL, Thorelius L, Holmqvist M, Bodemar G, and Kechagias S. Long-term follow-up of patients with NAFLD and elevated liver enzymes. *Hepatology* 44: 865–873, 2006.
14. Fassio E, Alvarez E, Dominguez N, Landeira G, and Longo C. Natural history of nonalcoholic steatohepatitis: a longitudinal study of repeat liver biopsies. *Hepatology* 40: 820–826, 2004.
15. Forbes LV, Sjogren T, Auchere F, Jenkins DW, Thong B, Laughton D, Hemsley P, Pairaudeau G, Turner R, Eriksson H, Unitt JF, and Kettle AJ. Potent reversible inhibition of myeloperoxidase by aromatic hydroxamates. *J Biol Chem* 288: 36636–36647, 2013.

16. Friedman SL. Hepatic stellate cells: protean, multifunctional, and enigmatic cells of the liver. *Physiol Rev* 88: 125–172, 2008.
17. Gabele E, Reif S, Tsukada S, Bataller R, Yata Y, Morris T, Schrum LW, Brenner DA, and Rippe RA. The role of p70S6K in hepatic stellate cell collagen gene expression and cell proliferation. *J Biol Chem* 280: 13374–13382, 2005.
18. Galli A, Svegliati-Baroni G, Ceni E, Milani S, Ridolfi F, Salzano R, Tarocchi M, Grappone C, Pellegrini G, Benedetti A, Surrenti C, and Casini A. Oxidative stress stimulates proliferation and invasiveness of hepatic stellate cells via a MMP2-mediated mechanism. *Hepatology* 41: 1074–1084, 2005.
19. Gressner AM, Weiskirchen R, Breitkopf K, and Dooley S. Roles of TGF-beta in hepatic fibrosis. *Front Biosci* 7: d793–d807, 2002.
20. Gujral JS, Hinson JA, Farhood A, and Jaeschke H. NADPH oxidase-derived oxidant stress is critical for neutrophil cytotoxicity during endotoxemia. *Am J Physiol Gastrointest Liver Physiol* 287: G243–G252, 2004.
21. Han D, Hanawa N, Saberi B, and Kaplowitz N. Mechanisms of liver injury. III. Role of glutathione redox status in liver injury. *Am J Physiol Gastrointest Liver Physiol* 291: G1–G7, 2006.
22. Ho JS, Buchweitz JP, Roth RA, and Ganey PE. Identification of factors from rat neutrophils responsible for cytotoxicity to isolated hepatocytes. *J Leukoc Biol* 59: 716–724, 1996.
23. This reference has been deleted.
24. Klebanoff SJ. Myeloperoxidase: friend and foe. *J Leukoc Biol* 77: 598–625, 2005.
25. Kleiner DE, Brunt EM, Van Natta M, Behling C, Contos MJ, Cummings OW, Ferrell LD, Liu YC, Torbenson MS, Unalp-Arida A, Yeh M, McCullough AJ, Sanyal AJ, and Nonalcoholic Steatohepatitis Clinical Research N. Design and validation of a histological scoring system for nonalcoholic fatty liver disease. *Hepatology* 41: 1313–1321, 2005.
26. Kluwe J, Pradere JP, Gwak GY, Mencin A, De Minicis S, Osterreicher CH, Colmenero J, Bataller R, and Schwabe RF. Modulation of hepatic fibrosis by c-Jun-N-terminal kinase inhibition. *Gastroenterology* 138: 347–359, 2010.
27. Lanza F. Clinical manifestation of myeloperoxidase deficiency. *J Mol Med (Berl)* 76: 676–681, 1998.
28. Leo MA and Lieber CS. Hepatic vitamin A depletion in alcoholic liver injury. *N Engl J Med* 307: 597–601, 1982.
29. Marra F, Arrighi MC, Fazi M, Caligiuri A, Pinzani M, Romanelli RG, Efsen E, Laffi G, and Gentilini P. Extracellular signal-regulated kinase activation differentially regulates platelet-derived growth factor's actions in hepatic stellate cells, and is induced by *in vivo* liver injury in the rat. *Hepatology* 30: 951–958, 1999.
30. Maschmeyer P, Flach M, and Winau F. Seven steps to stellate cells. *J Vis Exp* 51: pii: 2710, 2011.
31. Matteoni CA, Younossi ZM, Gramlich T, Boparai N, Liu YC, and McCullough AJ. Nonalcoholic fatty liver disease: a spectrum of clinical and pathological severity. *Gastroenterology* 116: 1413–1419, 1999.
32. Mello T, Nakatsuka A, Fears S, Davis W, Tsukamoto H, Bosron WF, and Sanghani SP. Expression of carboxylesterase and lipase genes in rat liver cell-types. *Biochem Biophys Res Commun* 374: 460–464, 2008.
33. Olaso E, Ikeda K, Eng FJ, Xu L, Wang LH, Lin HC, and Friedman SL. DDR2 receptor promotes MMP-2-mediated proliferation and invasion by hepatic stellate cells. *J Clin Invest* 108: 1369–1378, 2001.
34. Pulli B, Ali M, Forghani R, Schob S, Hsieh KL, Wojtkiewicz G, Linnoila JJ, and Chen JW. Measuring myeloperoxidase activity in biological samples. *PLoS One* 8: e67976, 2013.
35. This reference has been deleted.
36. Ratziu V, Charlotte F, Heurtier A, Gombert S, Giral P, Bruckert E, Grimaldi A, Capron F, Poynard T, and Group LS. Sampling variability of liver biopsy in nonalcoholic fatty liver disease. *Gastroenterology* 128: 1898–1906, 2005.
37. Reeves HL, Dack CL, Peak M, Burt AD, and Day CP. Stress-activated protein kinases in the activation of rat hepatic stellate cells in culture. *J Hepatol* 32: 465–472, 2000.
38. Reif S, Lang A, Lindquist JN, Yata Y, Gabele E, Scanga A, Brenner DA, and Rippe RA. The role of focal adhesion kinase-phosphatidylinositol 3-kinase-akt signaling in hepatic stellate cell proliferation and type I collagen expression. *J Biol Chem* 278: 8083–8090, 2003.
39. Reiniers MJ, van Golen RF, van Gulik TM, and Heger M. Reactive oxygen and nitrogen species in steatotic hepatocytes: a molecular perspective on the pathophysiology of ischemia-reperfusion injury in the fatty liver. *Antioxid Redox Signal* 21: 1119–1142, 2014.
40. Rensen SS, Bieghs V, Xanthoulea S, Arfianti E, Bakker JA, Shiri-Sverdlov R, Hofker MH, Greve JW, and Buurman WA. Neutrophil-derived myeloperoxidase aggravates nonalcoholic steatohepatitis in low-density lipoprotein receptor-deficient mice. *PLoS One* 7: e52411, 2012.
41. Rensen SS, Slaats Y, Nijhuis J, Jans A, Bieghs V, Driessen A, Malle E, Greve JW, and Buurman WA. Increased hepatic myeloperoxidase activity in obese subjects with nonalcoholic steatohepatitis. *Am J Pathol* 175: 1473–1482, 2009.
42. Rowell DL, Eckmann L, Dwinell MB, Carpenter SP, Raucy JL, Yang SK, and Kagnoff MF. Human hepatocytes express an array of proinflammatory cytokines after agonist stimulation or bacterial invasion. *Am J Physiol* 273: G322–G332, 1997.
43. Rudolph V, Andrie RP, Rudolph TK, Friedrichs K, Klinke A, Hirsch-Hoffmann B, Schwoerer AP, Lau D, Fu X, Klingel K, Sydow K, Didie M, Seniuk A, von Leitner EC, Szoecs K, Schrickel JW, Treede H, Wenzel U, Lewalter T, Nickenig G, Zimmermann WH, Meinertz T, Boger RH, Reichenspurner H, Freeman BA, Eschenhagen T, Ehmke H, Hazen SL, Willems S, and Baldus S. Myeloperoxidase acts as a profibrotic mediator of atrial fibrillation. *Nat Med* 16: 470–474, 2010.
44. Saeed AI, Sharov V, White J, Li J, Liang W, Bhagabati N, Braisted J, Klapa M, Currier T, Thiagarajan M, Sturn A, Snuffin M, Rezantsev A, Popov D, Ryltsov A, Kostukovich E, Borisovsky I, Liu Z, Vinsavich A, Trush V, and Quackenbush J. TM4: a free, open-source system for microarray data management and analysis. *Biotechniques* 34: 374–378, 2003.
45. Seki S, Kitada T, Yamada T, Sakaguchi H, Nakatani K, and Wakasa K. *In situ* detection of lipid peroxidation and oxidative DNA damage in non-alcoholic fatty liver diseases. *J Hepatol* 37: 56–62, 2002.
46. Selloum L, Djelili H, Sebihi L, and Arnhold J. Scavenger effect of flavonols on HOCl-induced luminol chemiluminescence. *Luminescence* 19: 199–204, 2004.
47. Singh R and Czaja MJ. Regulation of hepatocyte apoptosis by oxidative stress. *J Gastroenterol Hepatol* 22 Suppl 1: S45–S48, 2007.
48. Szabo C, Ischiropoulos H, and Radi R. Peroxynitrite: biochemistry, pathophysiology and development of therapeutics. *Nat Rev Drug Discov* 6: 662–680, 2007.

49. Takehara T, Tatsumi T, Suzuki T, Rucker EB, 3rd, Hennighausen L, Jinushi M, Miyagi T, Kanazawa Y, and Hayashi N. Hepatocyte-specific disruption of Bcl-xL leads to continuous hepatocyte apoptosis and liver fibrotic responses. *Gastroenterology* 127: 1189–1197, 2004.
50. Theruvath TP, Snoddy MC, Zhong Z, and Lemasters JJ. Mitochondrial permeability transition in liver ischemia and reperfusion: role of c-Jun N-terminal kinase 2. *Transplantation* 85: 1500–1504, 2008.
51. Tomita K, Tamiya G, Ando S, Ohsumi K, Chiyo T, Mizutani A, Kitamura N, Toda K, Kaneko T, Horie Y, Han JY, Kato S, Shimoda M, Oike Y, Tomizawa M, Makino S, Ohkura T, Saito H, Kumagai N, Nagata H, Ishii H, and Hibi T. Tumour necrosis factor alpha signalling through activation of Kupffer cells plays an essential role in liver fibrosis of non-alcoholic steatohepatitis in mice. *Gut* 55: 415–424, 2006.
52. Ventura JJ, Cogswell P, Flavell RA, Baldwin AS, Jr., and Davis RJ. JNK potentiates TNF-stimulated necrosis by increasing the production of cytotoxic reactive oxygen species. *Genes Dev* 18: 2905–2915, 2004.
53. Ward J, Spath SN, Pabst B, Carpino PA, Ruggeri RB, Xing G, Speers AE, Cravatt BF, and Ahn K. Mechanistic characterization of a 2-thioxanthine myeloperoxidase inhibitor and selectivity assessment utilizing click chemistry-activity-based protein profiling. *Biochemistry* 52: 9187–9201, 2013.
54. Weltman MD, Farrell GC, and Liddle C. Increased hepatocyte CYP2E1 expression in a rat nutritional model of hepatic steatosis with inflammation. *Gastroenterology* 111: 1645–1653, 1996.
55. Witek RP, Stone WC, Karaca FG, Syn WK, Pereira TA, Agboola KM, Omenetti A, Jung Y, Teaberry V, Choi SS, Guy CD, Pollard J, Charlton P, and Diehl AM. Pan-caspase inhibitor VX-166 reduces fibrosis in an animal model of nonalcoholic steatohepatitis. *Hepatology* 50: 1421–1430, 2009.
56. Yang L, Roh YS, Song J, Zhang B, Liu C, Loomba R, and Seki E. Transforming growth factor beta signaling in hepatocytes participates in steatohepatitis through regulation of cell death and lipid metabolism in mice. *Hepatology* 59: 483–495, 2014.
57. Zhang N, Francis KP, Prakash A, and Ansaldi D. Enhanced detection of myeloperoxidase activity in deep tissues through luminescent excitation of near-infrared nanoparticles. *Nat Med* 19: 500–505, 2013.
58. Zhao H, Kalivendi S, Zhang H, Joseph J, Nithipatikom K, Vasquez-Vivar J, and Kalyanaraman B. Superoxide reacts with hydroethidine but forms a fluorescent product that is distinctly different from ethidium: potential implications in intracellular fluorescence detection of superoxide. *Free Radic Biol Med* 34: 1359–1368, 2003.

Address correspondence to:
Prof. John W. Chen
Center for Systems Biology
Massachusetts General Hospital
and Harvard Medical School
185 Cambridge Street
Boston, MA 02114

E-mail: jwchen@mgh.harvard.edu

Date of first submission to ARS Central, August 31, 2014; date of final revised submission, May 1, 2015; date of acceptance, May 17, 2015.

Abbrevations Used

α-SMA = α-smooth muscle actin
ABAH = 4-aminobenzoic acid hydrazide
ERK = extracellular signal-regulated kinases
fMLP = N-formylmethionyl-leucyl-phenylalanine
GOX = glucose oxidase
H_2O_2 = hydrogen peroxide
HOCl = hypochlorous acid
HSC = hepatic stellate cell
JNK = c-Jun terminal kinase
LPS = lipopolysaccharide
MAPK = mitogen-activated protein kinase
MCD = methionine and choline deficient
MMP = matrix metalloproteinase
MPO = myeloperoxidase
$MPO^{-/-}$ = MPO knockout
MPT = mitochondrial permeability transition
NAFLD = nonalcoholic fatty liver disease
NASH = nonalcoholic steatohepatitis
P70S6K = 70-kDa ribosomal protein S6 kinase
PARP = poly (ADP-ribose) polymerase
PI3K = phosphoinositide 3-kinase
ROS = reactive oxidative species
TGF-β = transforming growth factor β
TNF = tumor necrosis factor
WT = wild-type